

Photoluminescence Spectroscopy of Cuprous Oxide: Bulk Crystal versus Crystalline Films

Mina Soltanmohammadi, Eleonora Spurio, Alexander Gloystein, Paola Luches, and Niklas Nilius*

Cuprous oxide (Cu_2O) crystals and films of 10–65 nm thickness are investigated via electron diffraction, scanning tunneling microscopy (STM), and photoluminescence (PL) spectroscopy at temperature between 100 to 300 K. While the chemical composition and surface morphology of both systems are identical, large differences are found in the optical response. Bulk Cu_2O shows pronounced PL peaks at 620, 730, and 920 nm, compatible with the radiative decay of free and bound excitons, whereas broad and asymmetric peaks at 775 and 850 nm are found for Cu_2O films grown on Au(111) and Pt(111) supports. The latter represent the PL signature of $V_{\text{O}^{2+}}$ and V_{O^+} defects, being inserted with substrate-dependent concentrations due to the oxygen-poor preparation of the Cu_2O films. Despite the strong V_{O} signature in PL, all Cu_2O samples show p-type conduction behavior in STM spectroscopy, indicating an abundance of Cu defects in the lattice. The fact that O vacancies still govern the thin-film PL is explained by a more efficient recombination via V_{O^-} than V_{Cu} -emission channels, as the latter requires exciton formation first. Herein, the high sensitivity of low-temperature PL to probe the defect landscape of dielectrics, being neither reached by photoelectron spectroscopy nor scanning probe techniques is demonstrated.

and imperfections in the 10^{-5} – 10^{-7} concentration range. Moreover, low-temperature PL provides information on the chemical nature, charge state, and atomic surrounding of the lattice imperfections. Phonon replicas give further insights into electron-vibrational coupling upon optical excitation. A fundamental problem of PL spectroscopy is the difficulty to link a luminescence fingerprint to a specific defect configuration, as no direct structural information is accessible.^[3] The assignment becomes feasible, however, if experimental emission data are compared to theoretical simulations performed for potential defect candidates.^[4] Respective calculations are demanding, as they require computation of excited electronic states, lattice relaxations, and many-particle effects to mimic exciton and trion formation.^[5] Not surprisingly, correlating low-temperature PL spectra to underlying atomic-scale defects remains challenging and has not been accomplished unambiguously even for prototype dielectrics, such as ZnO or GaN.^[3,6,7]

1. Introduction


Photoluminescence (PL) is a very sensitive detector for even small numbers of defects in dielectric solids.^[1,2] Whereas photoelectron spectroscopy is limited to defect concentrations of $\approx 1\%$ in the near-surface region, PL can safely detect impurities

and imperfections in the 10^{-5} – 10^{-7} concentration range. Moreover, low-temperature PL provides information on the chemical nature, charge state, and atomic surrounding of the lattice imperfections. Phonon replicas give further insights into electron-vibrational coupling upon optical excitation. A fundamental problem of PL spectroscopy is the difficulty to link a luminescence fingerprint to a specific defect configuration, as no direct structural information is accessible.^[3] The assignment becomes feasible, however, if experimental emission data are compared to theoretical simulations performed for potential defect candidates.^[4] Respective calculations are demanding, as they require computation of excited electronic states, lattice relaxations, and many-particle effects to mimic exciton and trion formation.^[5] Not surprisingly, correlating low-temperature PL spectra to underlying atomic-scale defects remains challenging and has not been accomplished unambiguously even for prototype dielectrics, such as ZnO or GaN.^[3,6,7]

This work deals with the unique optical response of cuprous oxide (Cu_2O).^[8] As a p-type conductor, Cu_2O plays an outstanding role among the binary oxides and is expected to be a main ingredient of all-oxide electronic devices in the future.^[9] Moreover, the Cu_2O bandgap of 2.15 eV locates in the middle of the visible spectrum, rendering this material interesting for photovoltaic and photochemical applications. Even bandgap gradients can be reproducibly fabricated by introducing gradual composition shifts from Cu_2O to CuO , the latter with 1.35 eV gap width.^[10] The optical properties of Cu_2O are governed by two excitonic modes and their trapping behavior to lattice defects.^[8,11] Both, the singlet-para and triplet-ortho excitons are characterized by long lifetimes, as the involved electrons and holes occupy Cu 4s conduction and Cu 3d valence states, respectively, making a direct optical decay parity forbidden. Radiative recombination of ortho excitons becomes possible, however, via phonon involvement and gives rise to a complex PL signature at ≈ 620 nm, comprising several phonon replicas and higher-order peaks.^[12–14] Moreover, Cu_2O excitons get trapped at various point defects in the oxide lattice, whereby Cu (V_{Cu}) and O vacancies ($V_{\text{O}^{2+}}$, V_{O^+}) produce the strongest in-gap peaks at 920, 730, and 840 nm, respectively.^[11]

Reported PL spectra of Cu_2O single crystals and, even more, of thin-film and powder samples exhibit a surprisingly high

M. Soltanmohammadi, A. Gloystein, N. Nilius
Institut für Physik
Carl von Ossietzky Universität
D-26111 Oldenburg, Germany
E-mail: niklas.nilius@uni-oldenburg.de
E. Spurio, P. Luches
CNR
Istituto Nanoscienze
Via G. Campi 213/a, 41125 Modena, Italy

 The ORCID identification number(s) for the author(s) of this article can be found under <https://doi.org/10.1002/pssa.202200887>.

© 2023 The Authors. physica status solidi (a) applications and materials science published by Wiley-VCH GmbH. This is an open access article under the terms of the Creative Commons Attribution-NonCommercial-NoDerivs License, which permits use and distribution in any medium, provided the original work is properly cited, the use is non-commercial and no modifications or adaptations are made.

DOI: 10.1002/pssa.202200887

variability. High-quality floating-zone crystals, for example, exhibit dominant V_{Cu} luminescence, in line with the high density of Cu defects expected for a p-type material.^[11,15] Natural crystals, in contrast, do not show V_{Cu} emission, although p-type conductivity has been reported also in this case.^[11,16] Moreover, the PL spectra of powder materials often comprise both V_{O} and V_{Cu} peaks, suggesting insufficient annihilation of majority and minority defects in the lattice.^[17–20] The free-exciton PL, on the other hand, is hardly detected in granular samples, as their low crystallinity collides with the long exciton lifetimes. In general, Cu_2O stoichiometry retrieval solely based on the Cu and O defect emission is challenging, as the underlying channels follow different excitation and recombination schemes and have different time and temperature dependencies.^[11,15,16] To obtain reliable insights into composition and defect structure of Cu_2O , the PL data needs to be complemented with other microscopic and spectroscopic techniques, providing additional information on the electronic structure and conductance behavior.^[21] We note that a precise control of the Cu_2O stoichiometry and defect landscape is crucial for optimizing the materials photovoltaic and photocatalytic response.^[9,22,23]

This study compares the temperature-dependent PL of a Cu_2O natural crystal with the one of Cu_2O films of variable thickness, grown on Au(111) and Pt(111) supports. While our low-energy electron diffraction (LEED), X-ray photoelectron spectroscopy (XPS), and scanning tunneling microscopy (STM) measurements indicate similar structural, electronic, and chemical properties of the examined samples,^[24,25] a deviating PL response suggests rather different defect landscapes. Our paper aims at correlating the specific PL of bulk and thin-film Cu_2O to an abundance of either copper or oxygen defects in the samples. We discuss whether the dominant V_{O} luminescence in the thin-film spectra conflicts with a p-type conductance that naturally relies on Cu-defects,^[26] and whether n-type Cu_2O can be synthesized at O-poor conditions.^[18,27] Finally, we address why plasmons at the metal/oxide interface do not contribute to the thin-film PL, although plasmonic light dominates the STM luminescence from 5 nm thick $\text{Cu}_2\text{O}/\text{Au}(111)$ films.^[28]

2. Results and Discussion

2.1. Thickness Determination of Cu_2O Films

The oxide films explored in this study have been prepared by high-pressure oxidation of vacuum-deposited Cu/Au(111) and Cu/Pt(111) layers, as discussed in the Experimental Section. A first requirement for correlating defect landscape and PL signature is a precise thickness determination of these films. We note that XPS cannot be used for this purpose, as the substrate peaks become invisible already at 10 nm film thickness, well below the range of interest in our study. We have therefore exploited thin-film interference techniques to follow the thickness evolution in subsequent deposition steps (Figure 1a). For this purpose, the sample reflectivity was probed with a white-light halogen lamp and normalized against a clean Pt(111) reference, as shown by the dark-blue line in Figure 1b. The reflectance curve exhibits a broad minimum at 665 nm, originating from destructive interference of light reflected from the Cu_2O surface and the $\text{Cu}_2\text{O}/$

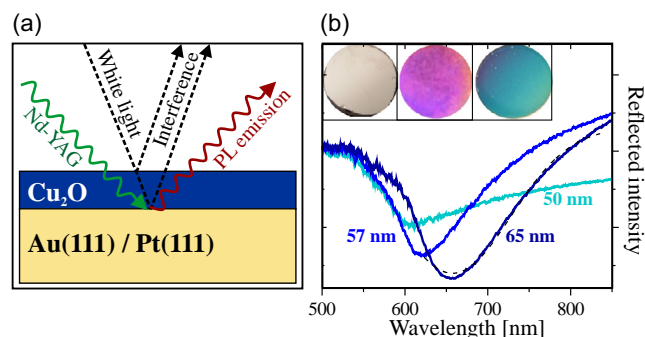


Figure 1. a) Sketch of the optical approach used in this work. The film thickness was derived from the 1st interference minimum of white light, the photoluminescence (PL) was stimulated by 532 nm laser photons. b) White-light reflectance of differently thick $\text{Cu}_2\text{O}/\text{Pt}(111)$ films. The inset shows photographs of pristine Pt(111) and after depositing 40 nm (middle) and 65 nm Cu_2O (right).

Pt(111) interface. The extinction condition is given by $2\sqrt{\epsilon_{\text{Cu}_2\text{O}} \cdot d \cdot \cos(\theta)} = m\lambda$ with $\epsilon_{\text{Cu}_2\text{O}} = 6.7$, the permittivity of the oxide layer,^[29] d the film thickness, $m = 1/2$ the phase factor of the 1st minimum and λ its wavelength. The $\cos(\theta)$ term is ≈ 1 , as incoming and outgoing beam closely follow the surface normal in our setup. For a minimum position at 665 nm, the procedure yields a film thickness of 65 nm.

The blue and cyan curves in Figure 1b depict similar interference data obtained for two other Cu_2O films. Apparently, the intensity minimum shifts to shorter wavelength, indicative for a decreasing film thickness. Simultaneously, the curves become asymmetric, as our white-light source lacks blue and violet components and the low-wavelength region thus gets suppressed in the spectra. To obtain approximate minimum positions also in this case, we have fitted the unperturbed, dark-blue curve with the Granfilm software that simulates the optical response of particle ensembles and thin films (Figure 1b, dashed line).^[30] The high-wavelength tails of the distorted spectra were now fitted with an identical data set, yet treating the film thickness as a parameter. By matching the resonance position in experiment and simulation, film thicknesses of 57 and 50 nm were obtained for the blue and cyan curve, respectively. These values are in good agreement with the number of deposition cycles conducted in our preparations, namely 6, 7, and 8 for the cyan, blue, and dark-blue curves, respectively. Apparently, each cycle adds 7–8 nm material to the existing film, which compares to ≈ 10 nm deposited Cu in each step. The discrepancy arises from Cu losses during oxidation and annealing, either due to evaporation or, more importantly, due to Cu alloying with the metal support. We note that 100% of the Cu would segregate into the Pt and Au crystal without chemical stabilization via oxidation, as discussed in our earlier work.^[31] Interestingly, the thin-film interference is strong enough to imprint a unique color change onto the metallic Pt(111) sample (Figure 1b, inset). After depositing a ≈ 40 nm thick film, the crystal adopts a pink color as only blue and red components of the incident light are reflected (central panel). The color changes to blue–green for a 65 nm thick film, as the yellow–red components are removed from the spectrum in that case (right panel).

2.2. Structure, Morphology, and Chemical Composition of Thin-Film versus Bulk Cu_2O

By exploiting the surface-science techniques available in our setup, we have investigated the lattice structure, chemical composition, and surface morphology of thin (111)-oriented Cu_2O films with respect to a (111) crystal. Photoelectron spectroscopy performed with an Al k -alpha source clearly reveal Cu_2O stoichiometry of both sample systems, as shown in the Supporting Information (SI).^[24,25] A quantitative analysis of the Cu 2p versus O 1s peak discloses a slight Cu deficiency of our films that becomes relevant later in the discussion. LEED measurements suggest an identical crystal structure of bulk and thin-film samples (Figure 2, insets). Both oxides exhibit a hexagonal symmetry with 6.1 Å lattice parameter, in perfect agreement with reported values for $\text{Cu}_2\text{O}(111)$.^[8] Moreover, $(\sqrt{3} \times \sqrt{3})R30^\circ$ superstructure spots are detected on their surfaces, being brighter and sharper for the bulk than the thin-film samples. A similar reconstruction was reported for (111)-oriented single crystals and films before,^[24,32,33] however, its atomic nature was only unraveled in a recent DFT study.^[34] In this model, every third Cu–O six ring of the regular (111) surface gets occupied by a Cu_4O nano-pyramid that saturates all oxygen dangling bonds. As a result, the surface energy is substantially reduced, which makes the nano-pyramidal reconstruction thermodynamically preferred over the stoichiometric and any other surface model proposed for $\text{Cu}_2\text{O}(111)$ so far.

The quality of the different Cu_2O surfaces was further assessed by high-resolution STM measurements (Figure 2). On all three oxide systems, wide and atomically flat terraces are found, in line with a perfect crystallinity of the underlying lattices. The terraces are homogeneously covered with a hexagonal ad-pattern of 10.5 Å periodicity, representing the nano-pyramidal reconstruction discussed before (Figure 2, insets). Each maximum reflects one Cu_4O nano-pyramid that even develops a distinct shamrock shape

at higher resolution.^[24] As already suggested from the LEED data, the $(\sqrt{3} \times \sqrt{3})R30^\circ$ reconstruction is better ordered on the bulk crystal, but can be recognized for Au(111)- and Pt(111)-supported Cu_2O films as well. At this point, we have no clue that the lower quality of the surface reconstruction is responsible for the different PL response of oxide films with respect to the bulk crystal, as detailed later in the text.

We have finally explored the valence electronic structure of thin-film versus bulk Cu_2O , using STM conductance spectroscopy (Figure 3). All three samples show a comparable spectral characteristic. A broad region of negligible dI/dV intensity, representing the oxide bandgap, gets enclosed by the valence (VB) and conduction band (CB) onset at 0 and +2.0 V, respectively. The corresponding gap size of ≈ 2.0 eV is identical for bulk and thin-film samples, and also in line with respective literature values.^[8] Moreover, the pinning of the VB top to the Fermi level manifests the p-type nature of Cu_2O and points to an abundance of acceptor-type V_{Cu} defects in the oxide matrix.^[26,27] The in-gap dI/dV peak at 0.3–0.5 V, clearly seen in the logarithmic representation, originates from tunneling into an empty-state pocket at the VB top. It arises from an upward bending of the surface bands due to the non-stoichiometric, that is, Cu-deficient nature of the pyramidal reconstruction, and is detected for all samples.^[35]

2.3. Luminescence Spectroscopy of Thin-Film versus Bulk Cu_2O

Figure 4 depicts normalized PL spectra of the bulk $\text{Cu}_2\text{O}(111)$ crystal, being stimulated with 532 nm photons of a NdYag laser and recorded for 60 s with a charge-coupled-device (CCD) detector. The optical response comprises three distinct bands at 620, 730, and 920 nm. The 920 nm peak clearly dominates the emission, while the low-wavelength maxima need to be multiplied by 20 to be plotted at the same scale. The intensity evolution as a function of temperature is derived from Gaussian fitting and displayed for all three peaks in Figure 4b. The high-wavelength peak at

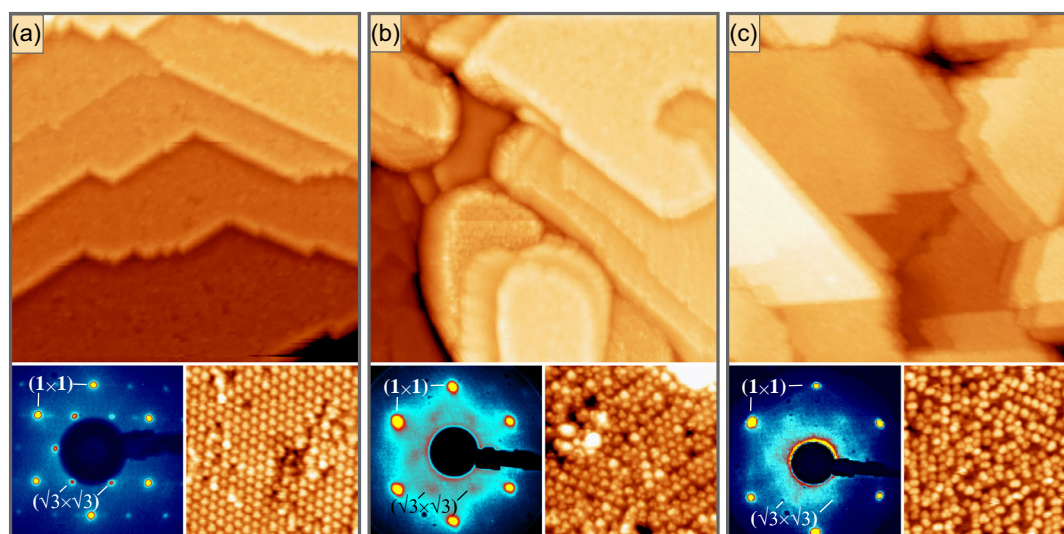


Figure 2. Overview and high-resolution STM topographic images of the $\text{Cu}_2\text{O}(111)$ surface of a) a single crystal, b) a 10 nm film grown on Au(111), and c) a 25 nm film on Pt(111) ($150 \times 150 \text{ nm}^2$, $U_{\text{B}} = 3.5 \text{ V}$, $I = 0.1 \text{ nA}$). All surfaces are homogeneously covered with Cu_4O nano-pyramids ($20 \times 20 \text{ nm}^2$, $U_{\text{B}} = -1.7 \text{ V}$, $I = 0.1 \text{ nA}$) that give rise to the $(\sqrt{3} \times \sqrt{3})R30^\circ$ reconstruction seen in the LEED measurements ($E_{\text{kin}} = 37 \text{ eV}$, insets).

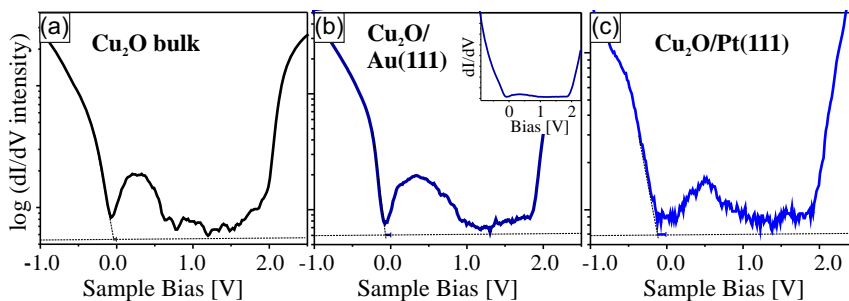


Figure 3. STM conductance spectra of a) bulk Cu_2O , b) 10 nm $\text{Cu}_2\text{O}/\text{Au}(111)$, and c) 25 nm $\text{Cu}_2\text{O}/\text{Pt}(111)$ shown on a logarithmic scale. The spectra were taken at 2.5 V set point bias and a starting current of a) 0.1 nA and b,c) 1 nA. The inset in (b) shows the same spectrum on a linear scale, demonstrating the low weight of the in-gap conductance with respect to direct tunneling into the oxide bands. The dotted lines mark the onsets of the Cu_2O valence band (VB).

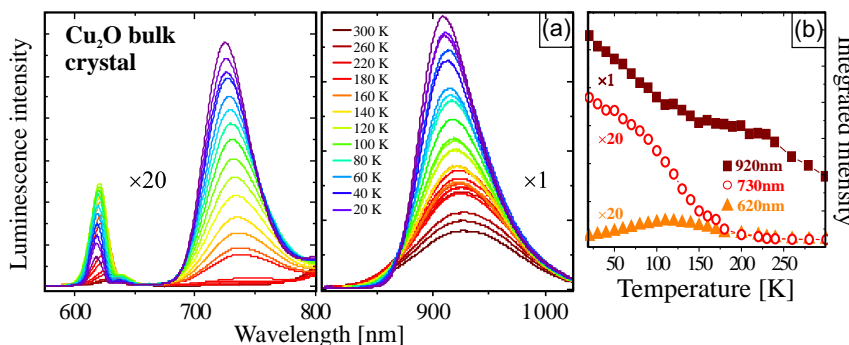


Figure 4. a) PL spectra of the Cu_2O bulk crystal. Given the dominance of the 920 nm peak, the spectrum is divided into two wavelength sections with different y-axis. b) Temperature dependence of the three PL maxima. Given the low intensity of the 620 and 730 nm peaks, their temperature curves have been multiplied by 20.

920 nm exhibits a steady intensity rise, whereas the 730 nm emission sets in only below 230 K and the 620 nm peak runs through a broad maximum at 125 K, decreasing again at lower temperature.

The PL signature of Cu_2O films on Au(111) and Pt(111) supports, measured at similar conditions, is plotted in **Figure 5**. While the $\text{Cu}_2\text{O}/\text{Au}(111)$ film has a height of ≈ 10 nm, the Pt(111)-supported film is ≈ 65 nm thick. The mean emission yield, calculated per nanometer, is however comparable in both cases and amounts to ≈ 100 photons $\text{s}^{-1} \text{nm}^{-1}$ at the peak maximum. The PL of Au-supported films exhibits an asymmetric shape, characterized by a sharp onset at 670 nm, a broad maximum at 775 nm, and a slow decay at higher wavelengths. In contrast, the $\text{Cu}_2\text{O}/\text{Pt}(111)$ luminescence is redshifted, with onset and peak position at 700 and 850 nm, respectively. Surprisingly, both data sets can be described by two Gaussians of similar position and width (Figure 5a,b, insets). While a low-wavelength peak at ≈ 750 nm (width 80 nm) governs the Au(111)-derived spectra, a high-wavelength maximum at ≈ 830 nm (width 100 nm) is dominant for the Pt(111)-supported films. The two spectral contributions show similar temperature dependence, being described by a gradual blueshift of the peak maximum and a steady intensity rise when cooling the samples to 100 K (Figure 5d). Panel 5c finally depicts the evolution of the $\text{Cu}_2\text{O}/\text{Pt}(111)$ luminescence as a function of film thickness. Evidently, the emitted intensity rises monotonously with film thickness, as compiled in the inset of panel 5c. The origin of the surprisingly different PL response of bulk and thin-film Cu_2O samples is addressed in the following section of our paper.

2.4. Nature of Thin-Film versus Bulk Cu_2O Luminescence

We start our discussion with the PL signature of bulk Cu_2O that is well documented in the literature.^[8,11,12] The three maxima observed in Figure 4a are consistently assigned to the radiative decay of free and bound excitons. The free-exciton emission is governed by the phonon-assisted decay of ortho-excitons, producing several sharp peaks centered at 620 nm.^[14] At the spectral resolution of our experiment, the individual phonon replicas are not resolved, but overlap to a single, asymmetric band. Its blueshift with decreasing temperature, reflecting the renormalization of the Cu_2O bandgap, is however discerned.^[36] The detected temperature evolution of the free-exciton peak also agrees with the reported behavior (Figure 4b, orange symbols).^[11] With decreasing temperature, the probability for radiative exciton decay rises, as thermal exciton scission into unbound electrons and holes becomes unlikely. This trend reverses at ≈ 125 K, when the ortho-excitons switch to non-radiative para-excitons that are more stable by 12 meV.^[37]

The peaks at 730 and 920 nm, in contrast, are assigned to Cu_2O excitons trapped at $\text{V}_{\text{O}^{2+}}$ and V_{Cu^-} vacancies, respectively.^[11,38] The two point defects introduce gap states localized below the CB edge (initial state in $\text{V}_{\text{O}^{2+}}$ decay) and above the VB top (final state in V_{Cu^-} decay), explaining the redshift of the respective emission peaks. The dominance of the V_{Cu^-} with respect to $\text{V}_{\text{O}^{2+}}$ emission is in line with the p-type nature of Cu_2O and reflects the thermodynamic preference to insert acceptor-type Cu vacancies into the lattice.^[26] The observed temperature

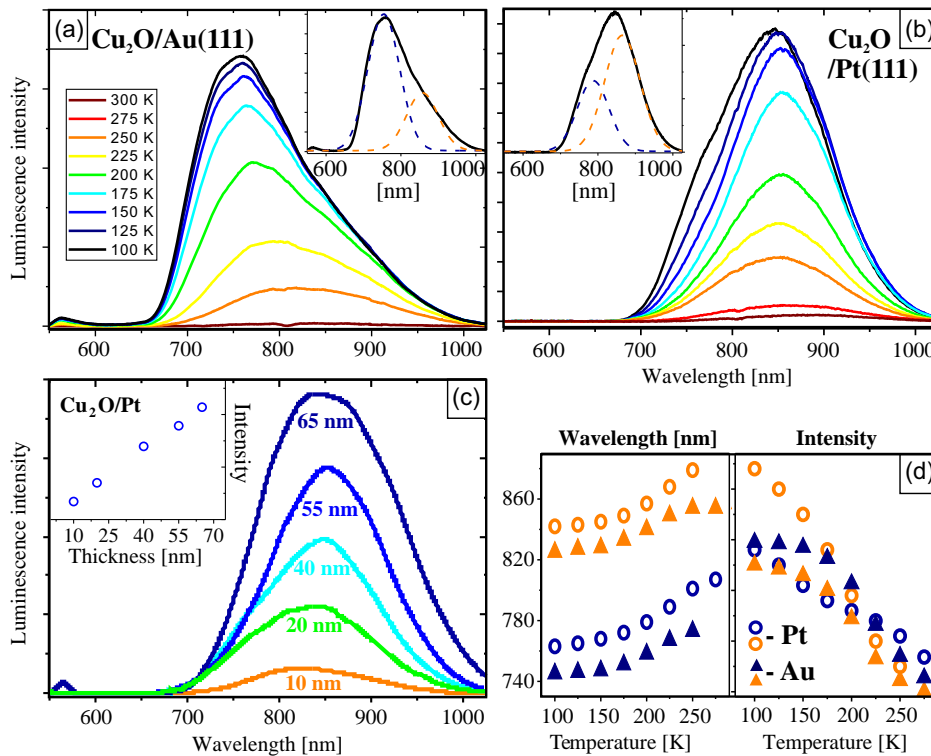


Figure 5. Normalized PL spectra taken with a 532 nm NdYag laser on a) 10 nm $\text{Cu}_2\text{O}/\text{Au}(111)$ and b) 65 nm $\text{Cu}_2\text{O}/\text{Pt}(111)$ films at different temperatures. c) Thickness-dependent PL data for $\text{Cu}_2\text{O}/\text{Pt}(111)$ films acquired at 100 K. The evolution of the integral emission intensity is plotted in the inset. d) Peak position and intensity of the two emission contributions that are required to fit the thin-film PL data, as shown in the insets of panels (a) and (b). Blue and orange symbols are for the short- and long-wavelength components, and open and closed symbols denote data for the Pt and Au support, respectively.

dependence of the 730 and 920 peaks further strengthens our assignment (Figure 4b, red and brown symbols). While the $V_{\text{O}^{2+}}$ related channels only opens below 230 K, as electrons are back-promoted from the defect state to the CB at higher temperature, the final state in the V_{Cu^-} transition gets blocked by thermal electrons from the VB at elevated temperature.^[11,38] The coexistence of Cu and O vacancies in the lattice finally indicates incomplete equilibration of the two main defect types in our bulk crystal.^[39]

Surprisingly, the luminescence of $\text{Cu}_2\text{O}(111)$ thin films seems incompatible with an exciton-mediated scheme, as neither the 620 nm peak related to free excitons nor the 920 nm peak arising from exciton trapping at V_{Cu^-} sites is observed. Moreover, the new PL band at ≈ 800 nm depends on the nature of the substrate, and redshifts when switching from Au(111) to Pt(111) supports (Figure 5). An obvious explanation for this behavior would be stimulation and radiative decay of surface plasmon polaritons (SPPs) that constitute light-driven collective electronic oscillations at the metal/oxide interface.^[40,41] To test this assumption, we have evaluated the plasmon dispersion at the $\text{Cu}_2\text{O}/\text{Au}(111)$ interface that follows: $k^2 = \left(\frac{\omega}{c}\right)^2 \frac{\epsilon_{\text{Cu}_2\text{O}} \epsilon_{\text{Au}}}{\epsilon_{\text{Cu}_2\text{O}} + \epsilon_{\text{Au}}}$ (Figure 6a). Here, $\epsilon_{\text{Cu}_2\text{O}}$ and ϵ_{Au} are the complex dielectric functions of the involved materials, k and ω are plasmon wavevector and frequency, and c is the speed of light.^[42] At the detected PL maximum of $\text{Cu}_2\text{O}/\text{Au}(111)$ (775 nm, Figure 5a), the plasmon wavevector calculates to $k_{\text{SPP}} = 0.7 \times 10^8 \text{ m}^{-1}$, which compares to a corresponding free-photon

wavevector of $k_{\text{ph}} = 0.22 \times 10^8 \text{ m}^{-1}$. This well-known wavevector mismatch of $\Delta k = 0.48 \times 10^8 \text{ m}^{-1}$ prohibits excitation and radiative decay of metal–oxide interface plasmons, unless it gets compensated by an auxiliary wavevector due to an optical grating or interface roughness.^[43] Our STM data of supported Cu_2O films shows however no indication for the requested periodicity ($2\pi/\Delta k \approx 130$ nm) and height corrugation ($70 \text{ nm} \approx 10\%$ of the photon wavelength) of such a grating (Figure 2b,c). Moreover, the detected temperature dependence of the thin-film PL cannot be reconciled with a plasmon-mediated emission mechanism. As similar conclusions also apply for Pt-supported films, we exclude that SPPs activated by interface roughness are responsible for the observed PL from Cu_2O thin films.

Conversely, PL bands in the 700–800 nm range were frequently reported in the literature for Cu_2O films, powders, and nanostructures.^[17,44] For example, Cu_2O films electrodeposited on ITO showed two distinct PL maxima at 775 and 885 nm, although no emission from free excitons and V_{Cu^-} defects was detected.^[18] Also, Cu_2O layers grown by magnetron sputtering revealed a distinct PL doublet at around 800 nm, again with little intensity in the wavelength region of the oxide excitons.^[29] A correlation between the 800 nm emission and the presence of O defects in the oxide lattice was first proposed by Zouaghi,^[16] and verified later by several control experiments. For example, while Cu_2O single crystals grown in a floating-zone scheme in air exhibit a strong 920 nm PL due to V_{Cu^-} defects, only the 730 nm peak is detected for crystals grown in Ar atmosphere.^[11]

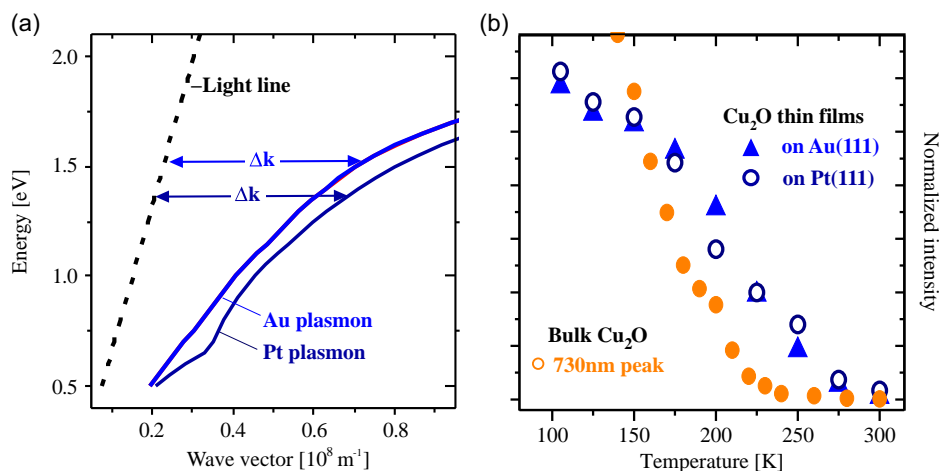


Figure 6. a) Dispersion relation of $\text{Cu}_2\text{O}/\text{Au}(111)$ (blue curve) and $\text{Cu}_2\text{O}/\text{Pt}(111)$ (dark-blue curve) interface plasmons in addition to the Cu_2O light line. The pronounced wavevector mismatch should be balanced by interface roughness, in conflict with the flat film morphology found in the STM images (Figure 2). b) Temperature dependence of the 730 nm peak area from bulk Cu_2O and the integrated PL intensity from the thin films.

Similarly, a strong $V_{\text{O}_2^+}$ peak emerges in nitrogen-doped Cu_2O samples, as the insertion of substitutional N_{O} is accompanied by the formation of oxygen defects.^[20] Theoretically, the $V_{\text{O}_2^+}$ emission from Cu_2O has been connected to an empty-state resonance at 1.53 eV above the VB edge that extends over the four Cu atoms adjacent to the vacancy.^[45] The resonance downshifts to 1.45 eV if one electron remains in the defect and a V_{O_+} complex is formed. According to HSE calculations, the $V_{\text{O}_2^+}$ defect becomes particularly stable if the Fermi level of Cu_2O locates directly at the VB top, while any E_{F} shift into the bandgap promotes generation of singly charged V_{O_+} defects. On this basis, we assign the unique emission doublet from our Cu_2O films to the PL fingerprint of O vacancies, whereby low- and high-wavelength components relate to double-charged ($V_{\text{O}_2^+}$) and single-charged (V_{O_+}) defects in the lattice, respectively.

2.5. Origin of the V_{O} Luminescence in Thin Films

The detection of two strong V_{O} -related PL peaks comes not unexpected in our experiments, as the Cu_2O preparation scheme is designed to be suitable for a vacuum UHV environment. Although an O_2 pressure as high as 50 mbar is used for initial Cu oxidation, the subsequent post-annealing step is performed in 10^{-4} mbar O_2 at 600 K, thus at reduced oxygen chemical potential (μ_{O_2}). We realized already in preceding studies that μ_{O_2} is the most sensitive parameter for oxide formation and insufficient availability of oxygen triggers Cu alloying with the support rather than oxidation to Cu_2O .^[31]

First insights into stoichiometry deviations between bulk and thin-film Cu_2O might be derived directly from the ratio of V_{Cu} versus V_{O} luminescence peaks. However, no Cu-vacancy emission was detected from our Au(111)- and Pt(111)-supported films, and the PL response of a dielectric material is actually a poor indicator for its defect landscape. Three reasons must be considered in the case of Cu_2O .^[15,46] 1) Defect luminescence in Cu_2O follows entirely different recombination pathways. The V_{O} emission is triggered by hot electrons generated upon

optical stimulation. Due to short-carrier lifetimes in Cu_2O , the decay process occurs on very short time scales (4 ps at low temperature) and is therefore insensitive to competing non-radiative decay channels.^[15] The V_{Cu} emission, in contrast, gets initiated by the trapping of free excitons at Cu defects. The associated decay times are at least one order of magnitude longer than those of the V_{O} luminescence, reflecting the long lifetime of the dipole-forbidden Cu_2O excitons. Given this excitation asymmetry, the thin-film luminescence is primarily governed by O defects that enable fast and effective decay upon optical stimulation, while the V_{Cu} emission relies on long-lived excitons, making it susceptible to structural disorder and non-radiative decay channels. 2) Each defect channel in Cu_2O comes with its own temperature dependence, which favors V_{Cu} emission at high but V_{O} emission at low temperature. And, 3) especially the V_{Cu} luminescence involves multi-phonon emission with large Huang–Rhys factors, lowering the emission yield. All three factors prohibit quantitative insights into V_{Cu} versus V_{O} concentrations alone from the intensity ratio of the respective PL peaks.

In a second approach, we have therefore performed XPS measurements on $\text{Cu}_2\text{O}/\text{Au}(111)$, $\text{Cu}_2\text{O}/\text{Pt}(111)$ and the bulk crystal to analyze the defect characteristics of the respective lattices (see Figure S1, Supporting Information). To estimate the overall oxide stoichiometry, we have divided the peak areas of Cu $2p^{3/2}$ (935 eV) and O 1s (530.5 eV) core levels after correcting them for their atomic sensitivity factors. We found a generally higher Cu deficiency in the oxide films as compared to the bulk crystal, in conflict with our expectations. However, these findings do not imply a lower concentration of O vacancies in the films, as charge transfer between support and interfacial O atoms and small CuO inclusions also contribute to the detected Cu deficiency. Among the two films, the Au(111)-supported one has lower Cu content than its Pt counterpart, which becomes relevant when discussing details of the PL spectra later in this chapter. The observed Cu deficiency of both thin-film and bulk Cu_2O emphasizes the robust p-type nature of cuprous oxide. It is also in line with the STM conductance data presented in Figure 3, where an E_{F} position at the VB top and the presence of an

empty-state VB pocket provide clear evidence for the p-type character of all three samples. In other words, a strong V_O luminescence combined with missing V_{Cu} emission is by no means a proof for an n-type nature of a Cu_2O sample, although similar conclusions have been made in the literature.^[18] The predominant V_O signal only points to a different balance between defect-mediated and non-radiative decay channels in our supported films compared to the bulk Cu_2O crystal that is of higher structural quality. We note that in line with the present study, the suppression of free-exciton and V_{Cu} luminescence is a common observation for Cu_2O powders and thin films and frequently reported in the literature.^[17,18,29,44]

Particularly interesting in our work is the dominance of the 830 over the 750 nm PL peak for Pt(111)-supported Cu_2O films, whereas the intensity ratio reverses for the Au(111) support. As discussed before, the two maxima arise from radiative electron decay via single-charged (V_{O+}) and double-charged (V_{O2+}) oxygen vacancies that develop different defect states in the oxide bandgap.^[45] Their charge state is actually controlled by a low-lying state that is in resonance with the oxide VB. While in the V_{O2+} complex, the two electrons left behind by a neutral desorbing O atom are annihilated by two holes from the p-type oxide, and one electron remains trapped in the V_{O+} complex. The thermodynamic stability of V_{O2+} with respect to V_{O+} defects is therefore governed by the hole concentration in the oxide, hence by the oxide Fermi level. For E_F positions directly at the VB top (high hole density), formation of V_{O+} defects is unfavorable with respect to V_{O2+} complexes, while more V_{O+} defects develop for E_F positions inside the bandgap.

With this information, the different defect landscapes in Au(111)- and Pt(111)-supported Cu_2O films can be explained. Oxide growth on Au(111) intrinsically results in high Cu deficiency, which arises from the strong incentive of copper–gold alloy formation due to similar structural, electronic, and chemical properties of both metals.^[47] The Au(111) surface thus acts as a sink for deposited copper, making interfacial mixing and oxide formation two highly competitive channels. Conversely, Pt shows a lower tendency for alloy formation and some unreacted Cu always accumulates at the Pt(111)– Cu_2O interface, serving as Cu source during film growth.^[31] As a consequence, the Au(111)-supported films typically show higher Cu deficiency, yet better p-type conductivity and lower E_F position than their Pt(111) counterparts. This gets reflected in a stronger V_{O2+} than V_{O+} emission from $Cu_2O/Au(111)$ films, while the ratio inverts for $Cu_2O/Pt(111)$ in good agreement with our data. Being aware of intrinsic uncertainties in STM conductance spectroscopy, this conclusion is also supported by the dI/dV spectra presented in Figure 3. While the energy separation between VB top and E_F is ≈ 0.1 eV for $Cu_2O/Au(111)$, it increases to 0.2 eV for $Cu_2O/Pt(111)$, making the latter system less Cu deficient, hence more susceptible to V_{O+} formation.

Our final paragraph addresses the temperature evolution of the V_O peak intensities in bulk and thin-film Cu_2O , as displayed in Figure 6b. Although the two curves follow a similar behavior, they do not coincide. While the emission onset is at 230 K for the bulk crystal, it upshifts to 270 K for the thin films. We suggest a physical origin of the discrepancy, although a systematic error due to the lower thermal conductivity of bulk oxides with respect to metallic samples cannot be excluded. The temperature

dependence of PL is generally governed by the competition of radiative and non-radiative decay channels, such as phonon or thermal electron excitations. It now appears plausible that this interplay is different for bulk and thin-film oxides, whereby deviations may arise from phonon softening, as found in MgO and CaO films,^[48,49] or strain-induced weakening of the dipole selection rules in the Cu_2O films. Although a detailed analysis of the phenomenon is beyond the scope of this paper, it might warrant a closer inspection in future.

3. Conclusions

PL measurements have been performed on bulk and thin-film Cu_2O samples over a wide temperature range. While the luminescence of bulk Cu_2O is governed by the radiative decay of free excitons and excitons trapped at Cu and O vacancies, only the V_O -mediated emission channel prevails in Cu_2O films. The unique PL signatures of bulk and thin-film oxides have been connected to their different defect landscapes. Although Cu defects are abundant in both systems, as concluded from their robust p-type conduction behavior, the oxide films exhibit a larger V_O concentration due to their vacuum-compatible preparation scheme that includes a final annealing step in 10^{-4} mbar O_2 . In addition, the V_O -mediated emission channel is less sensitive to structural disorder, favoring this recombination pathway in the thin films. Also, the metal substrate used for oxide growth affects the defect landscape and Au(111)-supported films have higher Cu deficiency (more V_{O2+} complexes) than their Pt(111)-grown counterparts (more V_{O+} complexes). Future experiments shall clarify whether the distinct V_O emission can be recorded also locally by STM luminescence spectroscopy.^[28] This would open a pathway to probe individual O defects, that is, the local O deficiency in the Cu_2O surface, directly in a spatially resolved experiment.

4. Experimental Section

The experiments were performed in an ultrahigh vacuum chamber ($p \approx 2 \times 10^{-10}$ mbar) equipped with standard surface–science tools for sample cleaning (Ar^+ sputtering, annealing), thin-film preparation (high-pressure oxidation, physical vapor deposition), and analysis (XPS, LEED, LN_2 -cooled STM). An attached optical setup enabled in situ PL and white-light reflectivity measurements in a temperature range of 100–300 K, performed with a NdYag laser (20 mW power) and a halogen lamp, respectively. PL data at temperatures down to 10 K could be measured in an external He-cooled cryostat. As the Cu_2O films underwent irreversible changes of their interface and surface morphology during air transfer, low-temperature data were only acquired from the bulk crystal. In either case, the optical response was detected with a LN_2 -cooled, single-line CCD detector attached to a grating spectrograph with 150 lines mm^{-1} .

Cuprous oxide films of arbitrarily thickness were prepared in a three-step procedure:^[24] 1) physical vapor deposition of 10 nm metallic Cu (purity 99.9%) either onto Au(111) or Pt(111) surfaces, cleaned by sputtering and annealing before; 2) oxidation in a designated high-pressure cell at 50 mbar O_2 and 450 K; 3) low-pressure annealing in front of a pin-hole doser ($p_{O_2} = 10^{-4}$ mbar) at 600 K to stimulate film crystallization. The procedure was repeated until the desired film thickness between 10 and 65 nm was reached. The Au(111) and Pt(111) substrates were selected for oxide growth, as their (2×2) surface cells closely matched the lattice parameter of bulk $Cu_2O(111)$, resulting in smooth metal–oxide interfaces. The $Cu_2O(111)$ bulk crystal, purchased from Surface Preparation

Laboratory, was prepared by Ar⁺ sputtering and vacuum-annealing at 800 K until a sharp LEED pattern was detected.^[25]

Supporting Information

Supporting Information is available from the Wiley Online Library or from the author.

Acknowledgements

M.S. and E.S. contributed equally to this work. M.S. and N.N. gratefully acknowledge financial support from the DFG grant Ni 650-5/2 “Functionalization of Cuprous Oxide: From Tailoring the Optical Response to Cu-based Ternary Oxide Materials.”

Open Access funding enabled and organized by Projekt DEAL.

Conflict of Interest

The authors declare no conflict of interest.

Data Availability Statement

The data that support the findings of this study are available from the corresponding author upon reasonable request.

Keywords

bulk versus thin films, Cu defects, cuprous oxide, O vacancies, photoluminescence

Received: December 17, 2022

Revised: January 28, 2023

Published online: March 23, 2023

- [1] B. Henderson, G. F. Imbusch, *Optical Spectroscopy of Inorganic Solids*, Clarendon, Oxford **1989**.
- [2] C. D. Geddes, *Reviews in Fluorescence*, Springer International Publishing, Cham **2017**.
- [3] A. Galdamez-Martinez, G. Santana, F. Guell, P. R. Martinez-Alanis, A. Dutt, *Nanomaterials* **2020**, *10*, 857.
- [4] C. Freysoldt, B. Grabowski, T. Hickel, J. Neugebauer, G. Kresse, A. Janotti, C. G. van de Walle, *Rev. Mod. Phys.* **2014**, *86*, 253.
- [5] P. Rinke, A. Schleife, E. Kioupakis, A. Janotti, C. Roedel, F. Bechstedt, M. Scheffler, C. G. van de Walle, *Phys. Rev. Lett.* **2012**, *108*, 126404.
- [6] C. Klingshirn, J. Fallert, H. Zhou, J. Sartor, C. Thiele, F. Maier-Flaig, D. Schneider, H. Kalt, *Phys. Status Solidi B* **2010**, *247*, 1424.
- [7] M. A. Reshchikov, H. Morkoc, *J. Appl. Phys.* **2005**, *97*, 061301.
- [8] B. K. Meyer, A. Polity, D. Reppin, M. Becker, P. Hering, P. J. Klar, T. Sander, C. Reindl, J. Benz, M. Eickhoff, C. Heiliger, M. Heinemann, J. Bläsing, A. Krost, S. Shokovets, C. Müller, C. Ronning, *Phys. Status Solidi B* **2012**, *249*, 1487.
- [9] A. Musa, T. Akomolafe, M. Carter, *Sol. En. Mater. Sol. Cells* **1998**, *51*, 305.
- [10] M. Balik, V. Bulut, I. Y. Erdogan, *Int. J. Hydrogen Technol.* **2019**, *44*, 18744.
- [11] T. Ito, T. Masumi, *J. Phys. Soc. Jap.* **1997**, *66*, 2185.
- [12] J. Thewes, J. Heckötter, T. Kazimierczuk, M. Aßmann, D. Fröhlich, M. Bayer, M. A. Semina, M. M. Glazov, *Phys. Rev. Lett.* **2015**, *115*, 027402.
- [13] T. Kazimierczuk, D. Fröhlich, S. Scheel, H. Stolz, M. Bayer, *Nature* **2014**, *514*, 343.
- [14] J. I. Jang, Y. Sun, B. Watkins, J. B. Ketterson, *Phys. Rev. B* **2006**, *74*, 235204.
- [15] L. Frazer, K. B. Chang, R. D. Schaller, R. K. Poeppelmeier, J. B. Ketterson, *J. Lumin.* **2017**, *183*, 281.
- [16] M. Zouaghi, B. Prevot, C. Carabatos, M. Sieskind, *Phys. Status Solidi A* **1972**, *11*, 449.
- [17] H. Solache-Carranco, G. Juárez-Díaz, A. Esparza-García, M. Briseño-García, M. Galván-Arellano, J. Martínez-Juárez, G. Romero-Paredes, R. Peña-Sierra, *J. Lumin.* **2009**, *129*, 1483.
- [18] R. Garuthara, W. Siripala, *J. Lumin.* **2006**, *121*, 173.
- [19] I. S. Brandt, C. A. Martins, V. C. Zoldan, A. D. C. Viegas, J. H. Dias da Silva, A. A. Pasa, *Thin Solid Films* **2014**, *562*, 144.
- [20] J. Li, Z. Mei, L. Liu, H. Liang, A. Azarov, A. Kuznetsov, Y. Liu, A. Ji, Q. Meng, X. Du, *Sci. Rep.* **2014**, *4*, 7240.
- [21] M. Nyborg, I. Kolevator, G. C. Vásquez, K. Bergum, E. Monakhov, *J. Appl. Phys.* **2021**, *130*, 175701.
- [22] M. Singh, D. Jampaiah, A. E. Kandjani, Y. M. Sabri, E. Della Gaspera, P. Reineck, M. Judd, J. Langley, N. Cox, J. Van Embden, E. L. H. Mayes, B. C. Gibson, S. K. Bhargava, R. Ramanathan, V. Bansal, *Nanoscale* **2018**, *10*, 6039.
- [23] M. G. Saber, R. H. Sagor, *Appl. Nanosci.* **2015**, *5*, 217.
- [24] A. Gloystein, N. Nilius, *J. Phys. Chem. C* **2020**, *124*, 28605.
- [25] A. Gloystein, J. Creed, N. Nilius, *J. Phys. Chem. C* **2022**, *126*, 16834.
- [26] H. Raebiger, S. Lany, A. Zunger, *Phys. Rev. B* **2007**, *76*, 045209.
- [27] D. O. Scanlon, G. W. Watson, *J. Phys. Chem. Lett.* **2010**, *1*, 2582.
- [28] A. Gloystein, N. Nilius, *New J. Phys.* **2021**, *23*, 093021.
- [29] J.-W. Park, H. Jang, S. Kim, S.-H. Choi, H. Lee, J. Kang, S.-H. Wei, *J. Appl. Phys.* **2011**, *110*, 103503.
- [30] R. Lazzari, I. Simonsen, *Thin Solid Films* **2002**, *419*, 124.
- [31] A. Gloystein, N. Nilius, *J. Phys. Chem. C* **2019**, *123*, 26939.
- [32] K. H. Schulz, D. F. Cox, *Phys. Rev. B* **1991**, *43*, 1610.
- [33] A. Önsten, M. Göthelid, U. O. Karlsson, *Surf. Sci.* **2009**, *603*, 257.
- [34] A. Gloystein, N. Nilius, J. Goniakowski, C. Noguera, *J. Phys. Chem. C* **2020**, *124*, 26937.
- [35] A. Gloystein, N. Nilius, *Phys. Status Solidi* **2021**, *258*, 2100337.
- [36] D. W. Snoke, A. J. Shields, M. Cardona, *Phys. Rev. B* **1992**, *45*, 11693.
- [37] J. T. Warren, K. E. O'Hara, J. P. Wolfe, *Phys. Rev. B* **1999**, *61*, 8215.
- [38] N. Harukawa, S. Murakami, S. Tamon, S. Ijuin, A. Ohmori, K. Abe, T. Shigenari, *J. Lumin.* **2000**, *87–89*, 1231.
- [39] G. P. Pollack, D. Trivich, *J. Appl. Phys.* **1975**, *46*, 163.
- [40] *Springer Series: Topics in Applied Physics* (Ed: S. Kawata), Springer, Berlin **2001**.
- [41] J. M. Pitarke, V. M. Silkin, E. V. Chulkov, P. M. Echenique, *Rep. Prog. Phys.* **2007**, *70*, 304207.
- [42] *Handbook of Optical Constants of Solids* (Ed: E. D. Palik), Acad. Press, Boston **1991**.
- [43] H. Raether, *Springer Tracts in Modern Physics*, Vol. 111, Springer, New York, NY **1988**.
- [44] P. R. Markworth, R. P. H. Chang, Y. Sun, G. K. Wong, J. B. Ketterson, *J. Mater. Res.* **2001**, *16*, 914.
- [45] C. Ricca, L. Grad, M. Hengsberger, J. Osterwalder, U. Aschauer, *Phys. Rev. Res.* **2021**, *3*, 043219.
- [46] L. Frazer, E. Lenferink, K. B. Chang, R. D. Schaller, R. K. Poeppelmeier, N. P. Stern, J. B. Ketterson, *J. Lumin.* **2015**, *159*, 294.
- [47] F. Grillo, H. Früchtl, S. M. Francis, N. V. Richardson, *New J. Phys.* **2011**, *13*, 013044.
- [48] L. Savio, E. Celasco, L. Vattuone, M. Rocca, P. Senet, *Phys. Rev. B* **2003**, *67*, 075420.
- [49] Y. Cui, S. Tosoni, W.-D. Schneider, G. Pacchioni, N. Nilius, H.-J. Freund, *Phys. Rev. Lett.* **2015**, *114*, 016804.